1　# Hot spots, hot moments, and spatiotemporal drivers of soil

2　# CO_2 flux in temperate peatlands using UAV remote sensing

3　Yanfei Li[1]*, Maud Henrion[1], Angus Moore[1], Sébastien Lambot[1], Sophie

4　Opfergelt[1], Veerle Vanacker[1], François Jonard[2†], Kristof Van Oost[1†]

5　[1] Earth and Life Institute, Université catholique de Louvain, 1348 Louvain-la-Neuve, Belgium.

6　[2] Earth Observation and Ecosystem Modelling Laboratory, SPHERES Research Unit, Université de

7　Liège, 4000 Liège, Belgium.

8　*Correspondence to: Yanfei Li (email: yanfei.li@uclouvain.be).

9　[†] These authors are co-last authors.

10

11 **Abstract**

12 CO_2 emissions from peatlands exhibit substantial spatial and temporal variability due to their

13 heterogeneous nature, presenting challenges to identify their underlying drivers and to accurately

14 quantify and model CO_2 fluxes. Here, we integrated field measurements with Unmanned Aerial Vehicle

15 (UAV)-based multi-sensor remote sensing to investigate soil respiration across a temperate peatland

16 landscape. Our research addressed two key questions: (1) How do environmental factors control the

17 spatial-temporal distribution of soil respiration across complex landscapes? (2) How do hot spots and hot

18 moments of biogeochemical processes influence landscape-level CO_2 fluxes? We find that dynamic

19 variables (i.e., soil temperature and moisture) play significant roles in shaping CO_2 flux variations,

20 contributing 43 % to seasonal variability and 29 % to spatial variance, followed by semi-dynamic

21 variables (i.e., NDVI and root biomass) (19 % and 24 %). Relatively static variables (i.e., soil organic

22 carbon (SOC) stock and C/N ratio) have a minimal influence on seasonal variation (2 %) but contribute

23 more to spatial variance (10 %). Additionally, predicting time series of CO_2 fluxes is feasible by using

24 key environmental variables (test set: $R^2 = 0.74$, $RMSE = 0.57$ µmol m^{-2} s^{-1}), while UAV remote sensing

25 is an effective tool for mapping daily soil respiration (test set: $R^2 = 0.75$, $RMSE = 0.54$ µmol m^{-2} s^{-1}). By

26 the integration of in-situ high-resolution time-lapse monitoring and spatial mapping, we find that despite

27 occurring in 10 % of the year, hot moments contribute 28 %–31 % of the annual CO_2 fluxes. Meanwhile,

28 hot spots—representing 10 % of the area—account for 20 % of CO_2 fluxes across the landscape. Our

29 study demonstrates that integrating UAV-based remote sensing with field surveys improves the

30 understanding of soil respiration mechanisms across timescales in complex landscapes, providing

31 insights into carbon dynamics and supporting peatland conservation and climate change mitigation

32 efforts.

33 **Keywords:** Peatlands, Soil respiration, Greenhouse gas (CO_2) emission, CO_2 hot spots, CO_2 hot

34 moments, Multi-sensor UAV remote sensing, Global warming

1 Introduction

Peatlands are globally distributed ecosystems that store approximately 600 Gt of carbon (Yu et al., 2010), despite covering less than 4 % of the Earth's land surface (Xu et al., 2018). However, rising concerns exist over peatlands shifting from carbon sinks to carbon sources due to the impact of climate change (Dorrepaal et al., 2009; Huang et al., 2021; Hopple et al., 2020), land use/cover conversion (Leifeld et al., 2019; Deshmukh et al., 2021; Prananto et al., 2020), and other disturbances (Wilkinson et al., 2023; Turetsky et al., 2015). In Europe, it has been reported that nearly half of the peatlands are suffering degradation, primarily due to drainage for agricultural or forestry activities (Leifeld et al., 2019; Unep, 2022). As a consequence, European peatlands currently emit up to 580 Mt CO_2-eq per year across the continent (Unep, 2022). Given the critical role of the peatland ecosystem in the terrestrial carbon cycle, it is therefore important to understand the mechanisms driving carbon fluxes and their responses to climate change and human disturbances.

Soil respiration in peatlands is influenced by a combination of biotic and abiotic factors, such as soil temperature and moisture (Treat et al., 2014; Fang and Moncrieff, 2001; Juszczak et al., 2013; Swails et al., 2022; Hoyt et al., 2019; Evans et al., 2021), vegetation and root biomass (Acosta et al., 2017; Wang et al., 2021), and soil organic matter quality (Hoyos-Santillan et al., 2016; Leifeld et al., 2012). CO_2 emissions from peatlands are highly variable over space and time, presenting challenges to accurately quantify and model carbon fluxes. This may partial because peatlands are characterized by a unique microtopography, including features such as soil branches and depressions (Moore et al., 2019). These small-scale variations create differences in hydrology, temperature, biogeochemistry, and vegetation (Harris and Baird, 2019), leading to substantial spatial differences in the factors that control CO_2 fluxes and the formation of hot spots with elevated CO_2 emissions (Kelly et al., 2021; Becker et al., 2008; Mcclain et al., 2003; Frei et al., 2012; Kim and Verma, 1992). For instance, the peat surface temperature differences within a 10 m x 10 m plot characterized by hummock and hollow features can be 20°C (Rhoswen et al., 2018). In addition, peatlands experience highly variable weather conditions, which can trigger periods of disproportionately high CO_2 fluxes—often referred to as 'hot moments'—in response to transient environmental changes, such as sudden shifts in temperature, rainfall events, or fluctuations in the water table (Anthony and Silver, 2023). High CO_2 emissions occur from discrete areas in space (hot spots) and over short periods (hot moments), and may disproportionately contribute to the overall

64   fluxes (Anthony and Silver, 2023; Fernandez-Bou et al., 2020).   Most studies have examined the

65   mechanisms and contributions of hot spots and hot moments of other greenhouse gases (N_2O, CH_4) in

66   agricultural and forestry ecosystems (Krichels and Yang, 2019; Anthony and Silver, 2021; Kannenberg

67   et al., 2020; Leon et al., 2014; Fernandez-Bou et al., 2020), while research on CO_2 emission hot spots

68   and hot moments in peatlands remains limited (Anthony and Silver, 2021, 2023).

69   Identifying and quantifying hot spots and hot moments in peatlands is challenging, requiring large-scale,

70   continuous, long-term observations. Currently, most studies on peatland soil respiration rely on point

71   measurements taken at intervals of half a month to one month, primarily during daytime (e.g., Wright et

72   al. (2013); Bubier et al. (2003); Kim and Verma (1992); Danevčič et al. (2010)). This spatiotemporal

73   limitation hinders the effective detection of hot spots and hot moments. Some studies attempted to

74   extrapolate point data using land-use maps (Van Giersbergen et al., 2024; Webster et al., 2008; Mcnamara

75   et al., 2008), but uncertainties in landscape-scale fluxes increase as the number of measurement locations

76   decreases (Arias-Navarro et al., 2017; Wangari et al., 2022; Wangari et al., 2023). While automated

77   chamber systems improve temporal resolution and help capture hot moments (Hoyt et al., 2019; Anthony

78   and Silver, 2023), they are typically limited to a few sampling points, and scaling up is constrained by

79   significant resource demands. Eddy covariance towers measure net ecosystem exchange over large areas

80   by recording high-frequency CO_2 concentrations and air turbulence, providing insights into temporal

81   variations at the ecosystem level (Rey-Sanchez et al., 2022; Abdalla et al., 2014). However, the

82   underlying controlling factors and mechanisms at the process level are difficult to infer due to the large

83   spatial footprint. In addition, they may not accurately represent the spatial heterogeneity of peatlands

84   (Lees et al., 2018). These limitations highlight the need for complementary approaches to estimate CO_2

85   fluxes at the landscape scale with methods adapted for heterogeneous peatland ecosystems.

86   Several studies have integrated satellite-based remote sensing datasets with on-site chamber

87   measurements to model landscape-scale CO_2 fluxes (e.g., Junttila et al. (2021); Wangari et al. (2023);

88   Lees et al. (2018); Azevedo et al. (2021)). Remote sensing datasets on topography and vegetation

89   parameters serve as proxies for soil moisture, vegetation cover, and nutrient availability, enabling large-

90   scale CO_2 emission estimates within peatlands (Lees et al., 2018). However, this approach is somewhat

91   limited by coarse spatial (10 m to 1 km) and temporal (1 to 16 days) resolutions, which may overlook

92   hot spots and hot moments, leading to potential over- or underestimations of CO_2 fluxes in heterogeneous

93   peatlands (Kelly et al., 2021; Simpson, 2023). This shortcoming might be overcome by using unmanned

94   aerial vehicles (UAVs) equipped with different kinds of sensors such as Red-Green-Blue (RGB),

95   multispectral, thermal infrared, and Light Detection and Ranging (LiDAR). UAVs offer flexible

96   deployment and capture high-resolution spatiotemporal data (1 cm to 1 m, minutes to months) (Minasny

97   et al., 2019) which makes them particularly suitable for monitoring complex peatland dynamics and

98   detecting hot spots and hot moments. Thus far, UAVs have proven to be reliable tools for peatland

99   applications, including vegetation mapping (Steenvoorden et al., 2023), topographic reconstruction

100   (Harris and Baird, 2019), peat depth and carbon storage estimation (Li et al., 2024), and moisture

101   monitoring (Henrion et al., 2025). In a recent study, Kelly et al. (2021) utilized UAV-derived land surface

102   temperature to estimate ecosystem respiration of a hemi-boreal fen in southern Sweden, and Pajula and

103   Purre (2021) and Walcker et al. (2025) employed UAV-based multispectral vegetation indices to map

104   ecosystem CO_2 flux at high resolution. These recent studies demonstrated the great potential of UAVs

105   for linking CO_2 fluxes with environmental factors at a very high resolution, although they mainly focused

106   on data from a single sensor. Few studies have explored the fusion of UAV-derived data from multiple

107   sensors for mapping soil respiration across peatland landscapes.

108   In this study, we integrate multi-sensor UAV-based remote sensing with traditional field surveys to

109   investigate soil respiration across a temperate peatland landscape, located in the Belgian Hautes Fagnes.

110   As one of the largest and most ancient peatlands in Western Europe, the Belgian Hautes Fagnes represents

111   an important ecosystem for studying peatland carbon fluxes due to its sensitivity to climate change and

112   hydrological dynamics. Our research addresses two key questions: (1) What controls the nature and

113   strength of the relationship between soil respiration and environmental factors across complex peatland

114   landscapes and across spatial-temporal scales? (2) How do hot spots or hot moments of biogeochemical

115   processes influence landscape-level carbon fluxes? More specifically, our study has three main objectives.

116   First, we aim to identify the factors driving seasonal and spatial variations in soil respiration. Second, we

117   assess the potential for linking environmental factors to CO_2 flux at high spatial and temporal resolutions.

118   Third, we discuss the timing and location of hotspots and hot moments, assessing their contributions to

119   overall CO_2 flux budgets.

2 Materials and methods

2.1 Study site

The Belgian Hautes Fagnes plateau, part of the Stavelot-Venn Massif, is located in eastern Belgium (Figure 1a). This elevated landscape experiences a humid climate, with mean annual air temperature and precipitation being approximately 6.7 °C and 1439.4 mm (period: 1971-2000), respectively (Mormal and Tricot, 2004). The peatlands in this region cover an area of 37.50 km^2, which primarily consist of raised bogs formed since the Late Pleistocene (Frankard et al., 1998). Our study site (50.49 N, 6.05 E; ~0.30 km^2) is located in the upper valley of the Hoëgne River peatland region (Figure 1a). The site is characterized by a distinct SE-NW oriented topographic gradient, with a clear transition from a low-relief plateau to steep hillslopes and then to the floodplain of a broad river valley (Sougnez and Vanacker, 2011). The area was drained and planted with spruces in 1914 and 1918. The plantations were progressively cleared between 2000 and 2016; since 2017, the site has been restored through reforestation with native hardwood species such as *Betula pubescens* and *Quercus robur*. Figure 1b shows main vegetation types across this landscape. An observation station of the Royal Meteorological Institute of Belgium (Mont Rigi, 50.51 N, 6.07 E) situated 3.0 km from the study site, records rainfall data every 10 minutes.
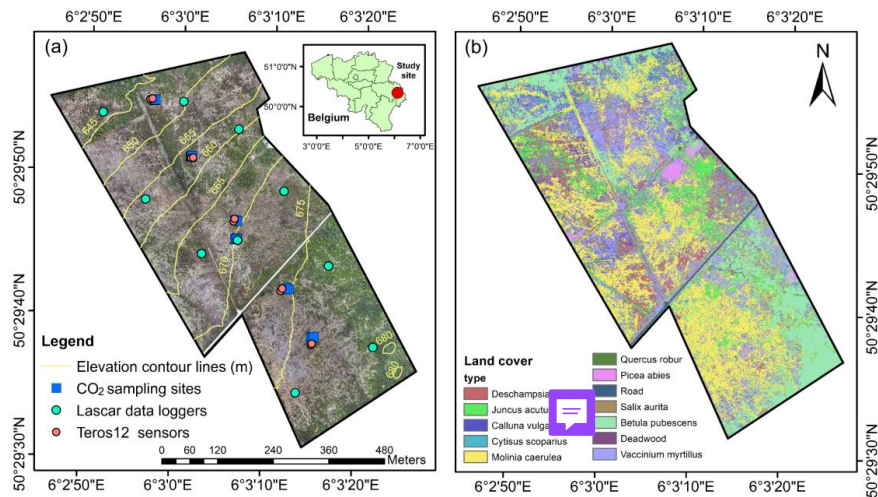
Figure 1. Maps showing the field-sampling locations (a) and land cover types (b) in the study area. Details on the land cover map are provided in our previous work (Li et al., 2024).

6

2.2 CO$_2$ flux measurement campaigns

Soil surface CO$_2$ flux measurements were conducted at five slope positions along the middle part of the site (Figure 1a). A portable infrared gas analyzer with an automated closed dynamic chamber (LI-8100A system, LI-COR, United States) was used to monitor CO$_2$ fluxes at 33 sites biweekly from December 2022 to March 2024 (Figure S1). At each slope position, six collars (20 cm diameter) were installed randomly, spaced 1–5 meters apart, to capture small-scale spatial variability. While at the boulder, considering the heterogeneous soil water conditions, six collars were installed in drier areas and another three in wetter areas. All vegetation within the collars was removed. During each campaign, monitoring was conducted between 9:00 and 16:00. At each site, the CO$_2$ flux (μmol m^{-2} s^{-1}) in the chamber was measured for 2.5 minutes per observation. Simultaneously, soil surface temperature (0–10 cm) and volumetric water content (VWC) during each CO$_2$ measurement were recorded using a T-handled type-E thermocouple sensor (8100-201, LI-COR, United States) and a portable five-rod, 0.06 m long frequency domain reflectometry (FDR) probe system (ML2x, Delta-T, United Kingdom), respectively. However, CO$_2$ measurements were not always possible due to technical issues and bad weather conditions, resulting in a total of 666 valid measurements. In addition, a pair of soil CO$_2$ forced diffusion probes (eosFD, EOSense, United States) were installed near LI-8100A collars from 24 April 2024 to 8 November 2024 (Figure S1). These probes, consisting of a soil node and a reference node, are based on a membrane-based steady-state approach and can measure CO$_2$ flux every 5 minutes (Risk et al., 2011). During this period, the probes continuously monitored CO$_2$ flux at different slope positions (Figure S1), resulting in a total of 39476 valid flux measurements.

2.3 Temperature and soil moisture monitoring

The temporal evolution of soil temperature and moisture along the middle part was monitored using Teros12 sensors (Meter Group, München, Germany), with two replicates per slope position, spaced 5 meters apart (Figure 1a) (Henrion et al., 2025). These sensors recorded data at a depth of 10 cm from 14 October 2022 to 28 October 2024, every 10 minutes. Between the two replicates of each slope position, a station positioned ~1.4 m above the ground recorded air temperature every ten minutes. Additionally, ten soil temperature data loggers (EL-USB-1-PRO, Lascar, United Kingdom) were installed primarily along two evenly spaced transects parallel to the main slope, at a depth of 10 cm (Figure 1a). These

167   loggers recorded soil temperatures at the same frequency as Teros12 sensors from 21 March 2023 to 8

168   November 2024.

169   **2.4 Soil sampling and laboratory analysis**

170   After completing all gas sampling campaigns, 33 disturbed soil samples (0-10 cm depth) were collected

171   within LI8100A collars at the five slope positions between 30 July and 15 October 2024. An Emlid Reach

172   RS 2 GPS device with centimeter-level precision was used to record the sampling site locations, using a

173   PPK solution with the Belgian WALCORS network. The samples were stored in a refrigerator until

174   laboratory analysis. A subset of the samples was oven-dried at 80 °C for 24 hours (Dettmann et al., 2021),

175   then crushed and ground into a fine powder for soil organic carbon (SOC) and total nitrogen content (TN)

176   analysis (928 Series, LEGO, United States). Roots and litter were removed using tweezers during the

177   pre-processing procedure. We tested the presence of inorganic carbon of each sample by adding one drop

178   of 10 % HCl but found that no inorganic carbon was present in the samples. A subset of fresh samples

179   was used for root biomass analysis. The fresh soil samples were weighed and placed in a 1 mm sieve,

180   then rinsed with water to collect the roots. The washed roots were dried in an oven at 80 °C for 48 hours

181   and then weighed to calculate their dry biomass.

182   **2.5 UAV data acquisition and imagery processing**

183   During the CO_2 flux monitoring period, we conducted regular UAV flights across the study area to collect

184   high-resolution spatial data (Figure S1). A DJI Matrice 300 RTK was equipped with four different sensors:

185   (i) a Red-Green-Blue (RGB) camera (DJI Zenmuse P1 camera, 35 mm and 45 MP), (ii) a multispectral

186   camera (MicaSense RedEdge-M camera with five discrete spectral bands: blue (475 nm), green (560 nm),

187   red (668 nm), rededge (717 nm), and near-infrared (842 nm), along with a downwelling light sensor),

188   (iii) a LiDAR scanner (DJI Zenmuse L1, integrated with a 20-MP camera with a 1-inch CMOS sensor)

189   and (iv) a thermal infrared camera (TeAX, featuring FLIR Tau2 cores and ThermalCapture hardware).

190   Similar flight patterns and altitudes were used for the UAV missions as in our previous work (Li et al.,

191   2024). In total, one RGB and one LiDAR dataset collected on 7 June 2023, were used in this study and

192   ten multispectral and ten thermal datasets collected between 13 April 2023 and 13 May 2024.

193   The raw multispectral images were processed in the Pix4D mapper software (Pix4D S.A., Lausanne,

194 Switzerland) to generate reflectance maps (resolution: 6 cm) of the five spectral bands of the study area.

195 We calculated the Normalized Difference Vegetation Index (NDVI) across the 10 maps from the

196 monitoring period (Table S1). The raw thermal infrared video streams were converted into RJPG images

197 using ThermoViewer version 3.0.26 (TeAX, 2022). Subsequently, the thermal images were processed

198 with the Pix4D mapper to generate land surface temperature (LST) maps (resolution: 12 cm), which were

199 used for soil temperature mapping (Text S1, Figure S2, Table S2). The RGB photos were processed in

200 DJI Terra V4.0.10 (DJI, 2023) to generate an orthomosaic image with a resolution of 1.26 cm. The raw

201 LiDAR data was processed in DJI Terra to provide a Digital Terrain Model (DTM; .tif file) with a

202 resolution of 15 cm, which was used for generating daily air temperature maps (Text S1) and terrain

203 wetness index (TWI) (Text S2). The variables derived from the four types of images were summarized

204 in Table S1.

205 2.6 Statistical analysis

206 All data analyses were conducted in RStudio (v4.1.2). All timestamps in this study were converted to

207 Coordinated Universal Time (UTC) to ensure consistency across datasets. Group differences were

208 assessed by the one-way analysis of variance (*ANOVA*) using the *stats package*. When *ANOVA* detected

209 a significant effect ($p < 0.05$), Tukey's Honestly Significant Difference (*HSD*) post-hoc test was

210 performed to determine which groups differed significantly from each other. Pearson correlation analysis

211 was performed using the *corrplot package* (Murdoch and Chow, 1996). The linear mixed-effects models

212 used to identify factors controlling spatial-temporal variations of CO_2 flux, as well as time series

213 simulation and mapping are introduced below.

214 2.6.1 Models to explain spatial-temporal variations in CO_2 flux

215 We utilized linear mixed-effects models to assess the impacts of both static and dynamic environmental

216 factors on the spatial and seasonal variability of CO_2 fluxes. This is because mixed models integrate both

217 fixed and random effects, which provide a robust framework for analyzing data with non-independent

218 structures (Pinheiro and Bates, 2000). The model was performed using the *lme4 package* (Bates et al.,

219 2015), with the natural logarithm of CO_2 flux observations as a response. The CO_2 fluxes data are often

220 characterized by extreme values and right-skewed distribution, and a lognormal assumption for CO_2

221   fluxes could better account for the influences of extreme values on the overall distribution (Wutzler et

222   al., 2020). The mixed-effects models were defined as:

223    $$y_{ij} = \beta_0 + \beta_1 x_{ij} + \cdots + \beta_p x_{ij} + b_{0j} + b_{1j} z_{ij} + \cdots + \epsilon_{ij} \qquad (1)$$

224   Where:

225   • y_{ij} is the dependent variable (i.e., ln (CO_2 flux), unit: μmol m^{-2} s^{-1}) for observations i in group

226   j.

227   • $\beta_0, \beta_1, \ldots, \beta_p$ are fixed-effect coefficients.

228   • x_{ij} is the fixed-effect variable (independent variable).

229   • b_{0j}, b_{1j},... are random-effect coefficients associated with group j, which account for

230   variability across groups.

231   • z_{ij} is the random-effect variable.

232   • ϵ_{ij} is the residual error term.

233   The fixed-effect predictors were categorized into three groups:

234   • Static variables: SOC stock, and the ratio of SOC content to nitrogen content (C/N ratio).

235   • Semi-dynamic variables: root biomass and NDVI.

236   • Dynamic variables: soil temperature and soil moisture at 0–10 cm depth.

237   Estimates for NDVI were extracted from the maps by retrieving the value of the 33 CO_2 flux observation

238   sites and the SOC stock values were extracted from the a local high resolution (0.15 m) SOC stock map

239   (Li et al., 2024). The sites were included as random effects in the seasonal pattern model to account for

240   repeated measurements at the same locations during the monitoring period, whereas slope positions were

241   treated as random effects in the spatial pattern model. Independent variable coefficients, Intraclass

242   Correlation Coefficient (*ICC*), coefficients of determination (*marginal R²* and *conditional R²*), Root Mean

243   Square Error (*RMSE*), and Akaike Information Criterion (*AIC*) were extracted using the *modelsummary*

244   *package* after running each model. The *ICC* quantifies the proportion of variance explained by a grouping

245   (random) factor in multilevel data; values close to 1 indicate high similarity within groups, while values

246   near 0 suggest that grouping conveys little to no information (Nakagawa et al., 2017; Shrout and Fleiss,

247   1979). The *marginal R²*, represents the variance explained by fixed effects alone, and *conditional R²*

248   represents the variance explained by both fixed and random effects (Pinheiro and Bates, 2000). The

249   relative importance of each independent variable was obtained using the *glmm.hp* package. To assess

250   multicollinearity in regression analysis, the *car package* was used to calculate the variance inflation

251   factor (*VIF*) (Fox and Monette, 1992).

2.6.2 Modelling hourly CO$_2$ flux

253   The mixed-effects model was utilized to simulate the time series of CO$_2$ fluxes at different slope positions.

254   Here, the slope position was included as random variable, and the natural logarithm of CO$_2$ flux (hourly)

255   was set as a response. We utilized CO$_2$ fluxes data measured by both the LI8100A system and eosFD

256   probes. Specifically, we randomly selected a number of 30 observations from the eosFD probes at each

257   slope position to reduce data redundancy from high-frequency sampling. Afterwards, we applied

258   weighting to adjust the remaining imbalance in data density between the high-frequency eosFD

259   monitoring and low-frequency LI8100A measurements, ensuring both data sources contributed

260   proportionally to the model. The independent variables included hourly soil temperature (10 cm depth),

261   volumetric soil moisture (VWC, 10 cm depth), and air temperature (1.4 m height), considering their

262   importance in explaining the seasonal and diurnal patterns of CO$_2$ flux.

263   As in our previous work (Li et al., 2024), we divided the dataset into a training set (70 %) and a test set

264   (30 %) using K-means clustering to minimize biases that could arise from random sampling (Hair et al.,

265   2010). The models were trained on the training set, and the simulation accuracy was validated using the

266   test dataset. The coefficient of determination (*R^2*) and *RMSE* were used to assess the quality of the model

267   fit. Finally, we made simulations of the time series of hourly CO$_2$ flux for different slope positions from

268   1 May 2023 to 30 April 2024. Furthermore, we identified CO$_2$ emission hot moments based on the

269   description in Section 2.6.4.

2.6.3 Mapping daily CO$_2$ flux

271   The linear mixed-effects model was utilized to map the spatial distribution of daily CO$_2$ fluxes across the

272   landscape, with daily soil temperature (10 cm depth), corrected daily TWI, and SOC stock being

273   considered as fixed-effect variables and gas sampling sites being included as random variables. The daily

274   CO$_2$ flux model training, testing procedures, and evaluation of model fit followed the same approach

275   detailed in Section 2.6.2. We then applied the trained model to predict the daily CO$_2$ flux of the landscape

276   from 1 May 2023 to 30 April 2024. Additionally, we calculated the mean daily soil CO_2 flux maps for

277   each season and the entire year. Based on these predictions, we identified hot spots for each day by the

278   methods described below.

2.6.4 Quantifying hot moments and hot spots of CO_2 flux

280   In previous studies, percentiles have been used as thresholds for identifying heat waves (e.g., (Meehl and

281   Tebaldi, 2004): 97.5th percentile), soil heat extremes (e.g., García-García et al. (2023): 90th percentile),

282   hot spots of N_2O emissions (e.g., Mason et al. (2017): median plus three times the interquartile range),

283   and hot spots of CO_2 emissions (e.g., Wangari et al. (2023): median plus the interquartile range). In this

284   study, we tested different methods and selected the 90th percentile as the threshold of both hot moments

285   and hot spots to balance capturing extreme CO_2 emissions while maintaining a sufficient sample size. To

286   capture the hot moments, we calculated a threshold for each slope position separately using its own

287   dataset. For hot spots, we determined a daily threshold based on each map.

288

3 Results

3.1 Spatial and temporal patterns of CO_2 flux

During the monitoring period, the CO_2 emissions show large spatial and seasonal variations across the landscape. The CO_2 fluxes at the summit (3.16 ± 3.25 µmol m^{-2} s^{-1}) and shoulder (dry: 2.81 ± 3.22 µmol m^{-2} s^{-1}, wet: 2.33 ± 2.36 µmol m^{-2} s^{-1}) slope positions were significantly higher than that of footslope (1.25 ± 1.00 µmol m^{-2} s^{-1}) and backslope (1.11 ± 1.03 µmol m^{-2} s^{-1}) ($p < 0.05$) (Figure 2a). Furthermore, significant differences were observed when grouping the data into three vegetation covers: CO_2 emissions from *Vaccinium myrtillus* were lower than those from *Juncus acutus*, with mean $\pm$ sd values of 1.59 ± 1.43 µmol m^{-2} s^{-1}, and 2.33 ± 2.36 µmol m^{-2} s^{-1}, respectively (Figure 2b) ($p < 0.05$). However, the CO_2 fluxes under *Molinia caerulea* displayed large variations ($0.02 \sim 20.1$ µmol m^{-2} s^{-1}), and no significant differences were found compared to the other two vegetation types. The CO_2 flux data indicated large CO_2 emissions from June to September (3.65 ± 2.68 µmol m^{-2} s^{-1}), which can be 8.11 times higher than that from winter and early spring (0.45 ± 0.40 µmol m^{-2} s^{-1}) (Figure 2c). CO_2 emissions in May and October were at a moderate level.
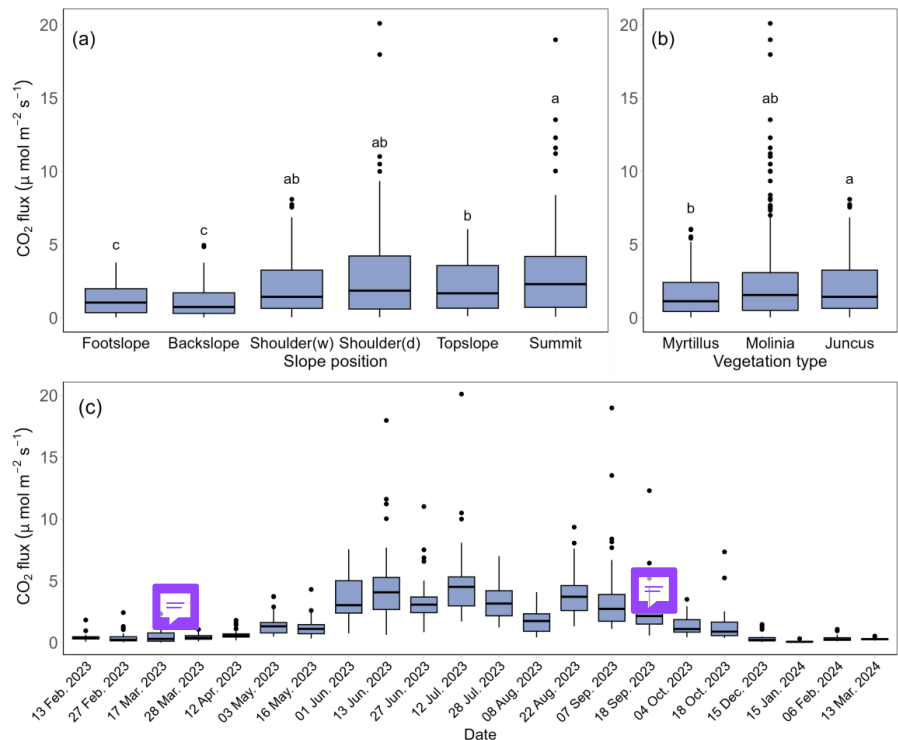
303

Figure 2. Boxplot of CO_2 flux (μmol m^{-2} s^{-1}) across different slope positions (a), vegetation types (b), and sampling

dates (c), using data from the LI8100 A system recorded between 2023-02-13 and 2024-03-13. (a), CO_2 flux data of

each box were from all dates, and Shoulder (w) and Shoulder (d) indicate shoulder wet and shoulder dry areas,

respectively. (b), CO_2 flux data of each box were from all dates, and Myrtillus, Molinia and Juncus indicate

Vaccinium myrtillus, *Molinia caerulea* and *Juncus acutus*, respectively. (c), CO_2 flux data of each box were from all

slope positions. The edges of each box represent the first quartile (Q1) and third quartile (Q3), while the line inside

the box indicates the median CO_2 flux. Whiskers extend from the box to the smallest and largest values within 1.5

times the interquartile range, and points outside the whiskers are considered extreme values. The *ANOVA* and *HSD*

post-hoc tests were performed within slope positions and vegetation types, with boxes sharing the same letters

indicating no significant difference.

3.2 Factors contributing to spatial-temporal variability

Three types of environmental factors explain 64 % of the observed seasonal variance in CO_2 emissions,

with contributions of 33 % from soil temperature, 10 % from VWC, 19 % from vegetation (i.e., NDVI,

14

317 root biomass), 2 % from relatively static factors (i.e., SOC stock, C/N ratio), and 6 % from random effects

318 (i.e., 33 sampling sites) (Table 1). This suggests that long-term stable environmental factors have minimal

319 direct influence on seasonal CO_2 flux patterns. Interestingly, the contribution of these relatively stable

320 factors is nearly 11 times higher in explaining overall spatial variations, although soil temperature is still

321 the dominant factor (Table 1). The low *ICC* values in both spatial and seasonal models highlight

322 significant small-scale heterogeneity in soil respiration.

323 **Table 1.** Coefficients and relative contributions of three types of input variables (static, semi-dynamic, dynamic) of

324 mixed linear regression models for modelling CO_2 flux. Random effects were evaluated by *ICC* and model

325 performance was evaluated by *Marginal R², Conditional R²,* and *RMSE.*

	Input variables		Seasonal patterns	Spatial patterns
Fixed effects: coefficient (contribution)	Static	SOC stock (t ha^{-1})	0.003 (1 %)	-0.003 (0.06 %)
		C/N ratio	0.05 (1 %)	0.07* (10 %)
	Semi dynamic	root biomass (g 100g^{-1})	0.06 (0.36 %)	0.09* (12 %)
		NDVI	0.90*** (18 %)	-3.35** (12 %)
	Dynamic	Soil temp. (°C)	0.12*** (33 %)	0.39*** (18 %)
		VWC (cm^3 cm^{-3})	-0.77*** (10 %)	-1.37** (11 %)
Random effects	*ICC* (contribution)		0.18 (6 %)	0.06 (3 %)
Model performance	*Marginal R²*		0.64	0.63
	Conditional R²		0.70	0.66
	AIC		1386.00	50.10
	RMSE		0.64	0.25

326 Note. Significance level: *** $p < 0.001$, ** $p < 0.01$, * $p < 0.05$. All CO_2 fluxes (unit: μmol m^{-2} s^{-1}), soil temperature,

327 and VWC data for spatial and seasonal patterns was from the LI8100 A system. To investigate the factors controlling

328 spatial variations of CO_2 flux, we calculated the mean values of CO_2 flux, NDVI, soil temperature, and VWC of

329 each site during the monitoring time.

3.3 Continuous hourly time series of CO₂ flux and hot moments

Three dynamic variables (i.e., soil temp., VWC, air temp.) were taken into account to predict the time series of hourly CO_2 flux at different slope positions. These input variables were selected due to their influential roles in explaining the diurnal (Figure S3) and seasonal fluctuations of CO_2 emissions. As shown in Table 2, the temporal model yielded a robust performance in both training and testing dataset, achieving R^2 and $RMSE$ values of 0.86 and 0.39 μmol m^{-2} s^{-1} and 0.74 and 0.57 μmol m^{-2} s^{-1}, respectively.

Table 2. Model performance for simulating time series of hourly CO_2 flux (unit: μmol m^{-2} s^{-1}) and mapping daily CO_2 flux (unit: μmol m^{-2} s^{-1}) across the landscape.

Models	Training dataset		Testing dataset	
	RMSE	R^2	*RMSE*	R^2
Temporal model	0.39	0.86	0.57	0.74
Spatial model	0.50	0.81	0.54	0.75

Note. Temporal model used the natural logarithm of CO_2 flux data from LI8100 A and eosFD probes, whereas spatial model used the natural logarithm of CO_2 flux data only from LI8100 A.

The modelled CO_2 emissions at all slope positions display a clear seasonal trend, with higher CO_2 fluxes from June to September and lower estimates in other months, in line with the observed fluxes shown in brown dots (Figures 3c-3h). The total CO_2 fluxes (Table 3) at the summit (19.50 t ha^{-1}) and the shoulder (dry: 19.47 t ha^{-1}, wet: 16.31 t ha^{-1}) slope positions were higher than that of topslope (14.45 t ha^{-1}), followed by footslope (13.94 t ha^{-1}) and backslope (11.54 t ha^{-1}) (Table 3), consistent with the spatial patterns of our observations (Figure 3a). However, the modelled mean ± sd CO_2 fluxes at all slope positions (Table 3) were lower than measured CO_2 fluxes by the LI8100 A system. This is because the measurements were taken during the daytime when fluxes were higher (Figure 2), whereas the modeled values represent the average of both daytime and nighttime fluxes. Most hot moments occurred from June to September 2023, whereas few hot moments were observed from late July to the early August (Figures 3c-3h). Although these hot moments of different slope positions only accounted for 10 % across the year, they could contribute 28 %-31 % to the annual total CO_2 emissions (Table 3).
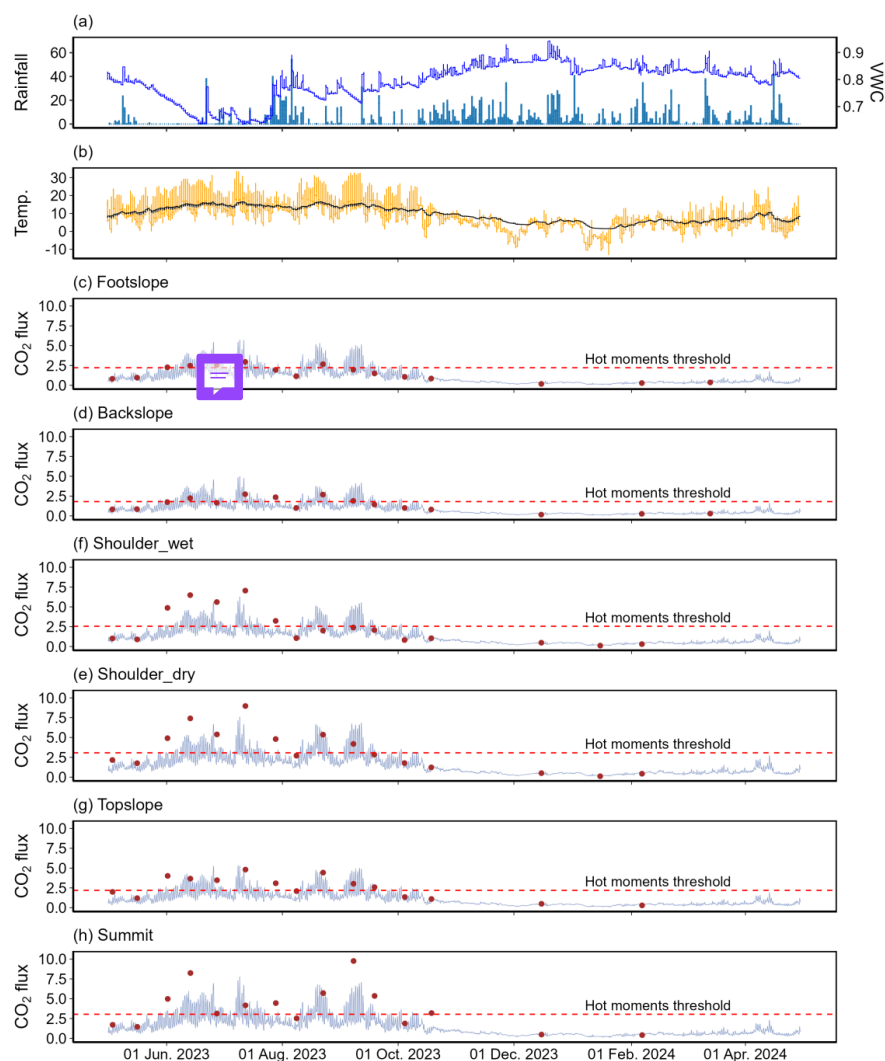
Figure 3. Time series of hourly rainfall (blue bar), hourly mean VWC (blue line) (a), hourly mean air temperature (orange line) and soil temperature (black line) (b), modelled hourly CO_2 flux (purple lines) and in-situ measurements (brown dots) at different slope positions (c-h). Rainfall (unit: mm) data was from the nearby meteorological observation station. The VWC (unit: cm^3 cm^{-3}) and soil temperature (unit: °C) were mean values from five slope positions monitored by Teros12 sensors at a depth of 10 cm. Air temperatures (unit: °C) were mean values from 5 stations at 1.4 m height above ground. Measured CO_2 fluxes (unit: μmol m^{-2} s^{-1}) were from the LI8100A system.

361   **Table 3.** Summary of modelled mean ± sd CO_2 fluxes, thresholds for identifying hot moments, total CO_2 flux, and

362   the contribution of hot moments to total flux at different slope positions.

Slope position	Footslope	Backslope	Shoulder wet	Shoulder dry	Topslope	Summit
Mean ± sd CO_2 flux (µmol m^{-2} s^{-1})	1.00 ± 0.91	0.83 ± 0.73	1.21 ± 0.99	1.44 ± 1.22	1.04 ± 0.86	1.41 ± 1.22
Total CO_2 flux (t ha^{-1})	13.94	11.54	16.31	19.47	14.45	19.50
Threshold (µmol m^{-2} s^{-1})	2.22	1.80	2.55	3.07	2.19	3.04
Contribution of hot moments	30.74 %	30.31 %	28.99 %	28.41 %	28.91 %	29.93 %

363   **3.4 Daily CO_2 flux maps and hot spots**

364   A linear mixed-effects model was utilized to map daily CO_2 flux from 1 May 2023 to 30 April 2024,

365   incorporating soil temperature, corrected TWI, and SOC stock as predictors due to their significant role

366   in explaining the spatial-seasonal variability of CO_2 flux and their availability as spatial data. The

367   mapping model yielded robust performance metrics (Table 2), with *R^2* and *RMSE* values of 0.81 and 0.50

368   µmol m^{-2} s^{-1} in the training dataset, and 0.75 and 0.54 µmol m^{-2} s^{-1} in the test dataset, respectively.

369   Consistent with our observations, the modelled soil respiration also displayed substantial spatial-

370   temporal heterogeneity (Figures 4a-4d). More specifically, the mean CO_2 fluxes ranged from 0.17 µmol

371   m^{-2} s^{-1} to 10.80 µmol m^{-2} s^{-1} in spring (Figure 4a), 0.36 µmol m^{-2} s^{-1} to 30.60 µmol m^{-2} s^{-1} in summer

372   (Figure 4b), 0.18 µmol m^{-2} s^{-1} to 14.87 µmol m^{-2} s^{-1} in autumn (Figure 4c), and 0.04 µmol m^{-2} s^{-1} to

373   2.24 µmol m^{-2} s^{-1} in winter (Figure 4d). Many modelled mean CO_2 fluxes at the footslope and backslope

374   (elevation < 660 m) remained below 2 µmol m^{-2} s^{-1} (Figure 4e). In contrast, the modelled CO_2 emissions

375   remained higher throughout the year at the shoulder (660 m ≤ elevation ≤ 670 m) and east of summit

376   (elevation > 675 m) with high vegetation cover. About 10 % of the area were identified as hot spots, with

377   a high frequency of hot spots occurring in these regions, while the locations of sporadic hot spots varied

378   over time (Figure 4f). Overall, the landscape emitted approximately 24.34 t ha^{-1} CO_2 to the atmosphere

379   during the simulation period, with 19.63 % ± 0.57 % of the CO_2 fluxes coming from the hot spots.

18
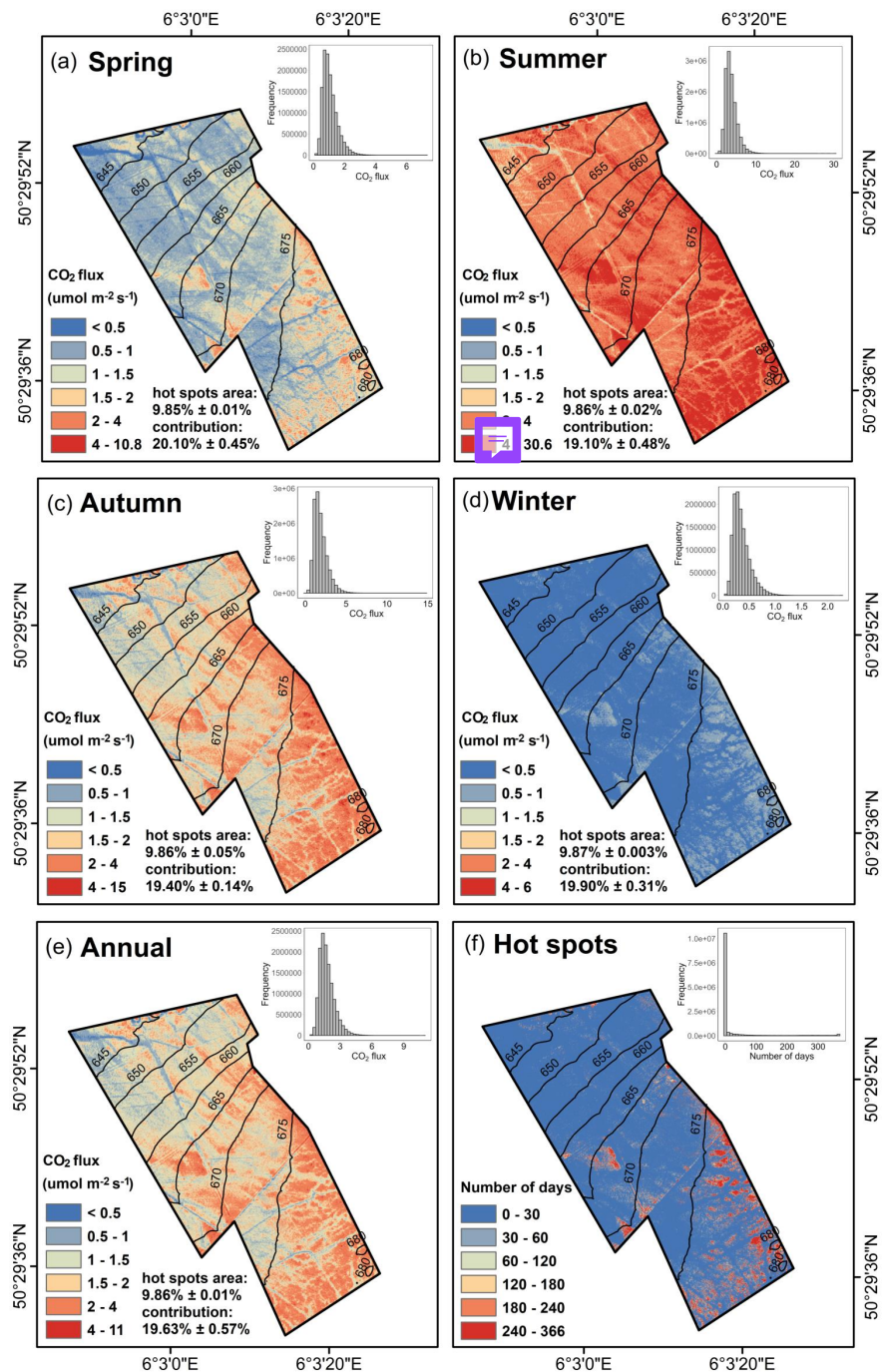
Figure 4. Maps of modelled mean daily CO_2 flux (μmol m^{-2} s^{-1}) in four seasons (a, b, c, d), throughout the year (e),

and hot spot frequency (f). The histograms of pixel values are presented on the top-right corner of each map. The

383   hot spots area proportion and CO_2 flux contribution from the hot spots of each season and across the year are

384   summarized in the corresponding maps.

4 Discussion

4.1 Drivers of spatiotemporal heterogeneity in CO_2 emission

Consistent with prior temperate peatland studies (Juszczak et al., 2013; Wilson et al., 2015; Danevčič et al., 2010; Swails et al., 2022), our results indicate that seasonal variations in soil CO_2 flux across the landscape are highly related to soil temperature, which could account for 33 % of the seasonal variability (Table 1). In contrast to tropical peatlands, where precipitation or water table fluctuations often dominate CO_2 flux dynamics (Hoyt et al., 2019; Cobb et al., 2017), our observations reveal that temperature exhibits distinct seasonal patterns (Figure 3b), which in turn drive fluctuations in soil respiration throughout the year (Figure 2c). Moreover, spatial heterogeneity in soil temperature further shaped landscape-scale CO_2 emission patterns (Table 1). For instance, the south-facing summit slopes, which receive more solar radiation in the daytime, consistently show higher CO_2 fluxes (Figure 2a). Conversely, the north-facing footslope and backslope, situated on the windward side, experience lower temperatures, resulting in generally lower soil respiration rates throughout the observation period (Figure 2a). While temperature is the dominant driver, soil water content influences oxygen availability within the peat profile, thereby regulating microbial decomposition and CO_2 production (Hatala et al., 2012; Knox et al., 2015; Zou et al., 2022; Huang et al., 2021; Deshmukh et al., 2021). For example, Knox et al. (2015) demonstrated that a declining water table caused by drainage increases oxygen penetration into the peat, resulting in higher CO_2 flux compared to restored peatlands. In our study case, the CO_2 fluxes were slightly higher in drier shoulder positions compared to wetter areas (Figure 2a), and VWC accounted for approximately 10 % of the spatial-seasonal variance in CO_2 fluxes (Table 1).

The monthly/biweekly NDVI is the second-most influential predictor for CO_2 seasonal fluctuations (Table 1), as NDVI reveals vegetation phenology during the monitoring period. In the spatial-pattern model, the contribution from root biomass becomes more substantial, together with mean NDVI explaining 24 % of spatial variance. These findings align with previous studies that vegetation mediates soil respiration through root respiration, exudates, litter inputs, and rhizosphere priming effects (Acosta et al., 2017; Wang et al., 2015a; Walker et al., 2016; Jovani-Sancho et al., 2021; Bragazza et al., 2013). In our study, the CO_2 fluxes of dwarf shrubs (i.e., *Vaccinium myrtillus*) were significantly lower than those in *Juncus acutus*-dominated areas (Figure 2b), likely due to the lower root biomass of dwarf shrubs

413   (Table S3). Furthermore, it has been shown that dwarf shrubs in northern peatlands produce high-

414   phenolic litter with higher resistance to breakdown and introduce more water-soluble phenolics into the

415   soil compared to *Sphagnum*/herbs (Bragazza et al., 2013; Wang et al., 2015a), which further constrains

416   microbial activity and CO_2 production. In addition, vegetation cover may indirectly influence soil

417   respiration by regulating surface microclimate conditions such as humidity and temperature (Nichols,

418   1998; Stoy et al., 2012).

419   As shown in Table 1, the SOC stock and C/N ratio have limited explanatory power for the seasonal

420   variability of CO_2 flux, in line with findings of Danevčič et al. (2010). However, when analyzing drivers

421   of average soil CO_2 flux rate across the entire monitoring period, the importance of C/N ratio increased

422   nearly 11 times (Table 1). This likely reflects how long-term averaging integrates short-term dynamic

423   variability, thereby amplifying the role of spatial heterogeneity mediated by the C/N ratio. Prior studies

424   suggesting that the quality of organic material, rather than its quantity, primarily regulates CO_2 fluxes in

425   peatlands (Hoyos-Santillan et al., 2016; Leifeld et al., 2012). Specifically, the soil C/N ratio is known to

426   regulate microbial community functionality and respiration intensity (Leifeld et al., 2020; Briones et al.,

427   2014; Ishikura et al., 2018; Wang et al., 2015b).

428   **4.2 CO_2 emission hot moments and hot spots: identification, implications, and importance**

429   **4.2.1 Temporal analysis and hot moments**

430   During past decades, efforts have been made to model CO_2 flux over time based on its relationship with

431   environmental factors such as hydrology, temperature, substrate quality, microbial community, and

432   vegetation (Hoyt et al., 2019; Junttila et al., 2021; Schubert et al., 2010; Rowson et al., 2012; Abdalla et

433   al., 2014; Farmer et al., 2011; Anthony and Silver, 2021). In our study, diurnal cycles of CO_2 fluxes are

434   closely related to air temperature (Figure S3), while soil temperature and moisture are important factors

435   in explaining the seasonal patterns of CO_2 flux (Table 1). Hence, the three dynamic environment variables

436   were incorporated into the model to simulate the hourly CO_2 flux across the entire monitoring period.

437   Overall, the temporal model demonstrated robust performance in both the training and testing datasets

438   (Table 2) and effectively captured seasonal and diurnal trends at most sites (Figures 3c-3h). However,

439   the modelled peak values are lower than the observations at shoulder and summit slope positions (Figures

440   3f, 3e, 3h), which may be partially due to the limited number of high-value observations in these areas.

441   Consequently, the model is more influenced by the more frequent lower CO_2 fluxes, leading to an overall

442   underestimation of the peak. In addition, two types of gas analyzers were employed to monitor CO_2 flux

443   with different sampling frequency and time: the LI-8100A sensor was used biweekly or monthly to

444   capture seasonal trends, while eosFD probes collected data every five minutes to track diurnal

445   fluctuations. The integration of these datasets for modelling temporal dynamics improved estimation

446   accuracy but might also introduce uncertainties into the model.

447   Anthony and Silver (2023) demonstrated that identifying hot moments of CO_2 flux in peatland requires

448   intensive continuous measurements, while as an alternative, our robust simulation of hourly CO_2 flux

449   enabled the identification of hot moments in a complex landscape. We found that most of these hot

450   moments occurred during the summer and early autumn seasons (Figure 3c-3h), in agreement with our

451   in-situ observations (Figure 2c). The frequent high CO_2 emissions in June and July can be attributed to

452   the low precipitation, decreased soil moisture, and high temperatures (Figure 3a-3b). However, few hot

453   moments were captured during late July and early August due to the heavy rainfall event (Figure 3a).

454   This absence may be attributed to the fact that intense rainfall led to lower temperatures and increased

455   soil moisture (Figures 3a, 3b), thereby suppressing microbial and root respiration (Hoyt et al., 2019).

456   Following this period, CO_2 emissions reached values that exceeded the 'hot moments' threshold in mid-

457   August, aligning with declining rainfall and rising temperatures (Figures 3c-3h). The hot moments

458   observed in September are linked to seasonal fluctuations in precipitation and temperature (Figures

459   3a,3b).

460   Similar to the findings of Anthony and Silver (2021) and Kannenberg et al. (2020), these hot moments

461   accounted for approximately 10 % throughout the year, while they contributed significantly to the annual

462   total CO_2 emissions (28 %-31 %; Table 3), highlighting the important role of short-term high-emission

463   events in the overall carbon emission. Therefore, missing hot moments may lead to significant

464   underestimates of total peat soil respiration budgets. Despite continuous automated chamber or eddy

465   covariance measurements that are ideal for capturing hot moments of CO_2 emissions (Anthony and Silver,

466   2023; Hoyt et al., 2019; Anthony and Silver, 2021), long-term continuous monitoring is still labor-

467   intensive and cost-prohibitive in many locations within the complex peatland ecosystems. Given that we

468   observed a concentration of hot moments in the summer and autumn, we recommend increasing

469   monitoring frequency during these seasons for temperate peatlands. This strategy would help capture

470   carbon emission dynamics more effectively, reduce uncertainties in annual carbon flux estimates, and

471   provide more representative peatland CO_2 flux data.

472   **4.2.2 Spatial analysis of CO_2 fluxes and hot spots**

473   Our mapping of CO_2 flux across the landscape yielded a model performance of $R^2 = 0.75$ and $RMSE =$

474   0.54 μmol m^{-2} s^{-1} for the test dataset (Table 2). This can be attributed to the incorporation of key

475   environmental factors that drive the spatiotemporal heterogeneity of soil respiration into the model inputs.

476   These factors – including soil temperature, corrected TWI, and SOC stock – can be directly obtained

477   through multi-sensor UAV remote sensing or estimated using high spatiotemporal resolution data.

478   Previous studies upscaled spatial carbon fluxes using area-weighted methods, extrapolating point data

479   from CO_2 chamber flux measurements to adjacent or larger areas based on land cover maps (Van

480   Giersbergen et al., 2024; Webster et al., 2008; Leon et al., 2014). However, this approach can lead to

481   over- or underestimation (Wangari et al., 2023; Leifeld and Menichetti, 2018), because our findings

482   reveal that even within the same vegetation cover, such as *Molinia caerulea*, CO_2 emissions exhibit

483   significant spatial-temporal variability (Figure 2b). In recent years, spatial upscaling of CO_2 fluxes has

484   increasingly relied satellite-based remote sensing data (e.g., Junttila et al. (2021); Wangari et al. (2023);

485   Zhang et al. (2020); Azevedo et al. (2021); Huang et al. (2015). While this method covers larger areas,

486   it is often constrained by coarse temporal and spatial resolutions. The peatland ecosystem is characterized

487   by great temporal and spatial heterogeneity at small scales, and ignoring these variations can introduce

488   significant uncertainties in CO_2 emission estimates. Our study demonstrates that high-resolution UAV

489   remote sensing imagery, with fine temporal and spatial scales, could effectively upscale CO_2 fluxes from

490   point measurements across a heterogeneous landscape, thereby reducing uncertainties in spatial

491   predictions of CO_2 fluxes.

492   Furthermore, the high-resolution CO_2 flux maps allowed for the identification of hot spot areas across

493   the landscape. We found that most of the hot spots occurred at the shoulder areas where soil moisture

494   was relatively lower and to the east of the summit which is covered by dense vegetation (Figure 1b,

495   Figure 4f). Spatial variability in the factors controlling biogeochemical processes, such as soil

496 temperature, moisture, water table depth, vegetation type, and substrate quality, is likely driving these

497 differences (Anthony and Silver, 2023; Kuzyakov and Blagodatskaya, 2015; Mcnamara et al., 2008). For

498 instance, the tree-covered areas at the summit contribute substantial root respiration, which may, in turn,

499 trigger the formation of consistent hot pots throughout the year. Besides, litterfall beneath trees insulates

500 the peat soil and provides an abundant resource for microbial activity.

501 High-emission events from hot spots play a crucial role in overall CO_2 fluxes (Anthony and Silver, 2023),

502 hence, neglecting these areas could lead to substantial underestimation of peatland carbon emissions. In

503 our study, although less than 10 % of area was identified as hot spots, their CO_2 flux contribution

504 accounted for nearly 20 % across the year (Figure 4). However, research specifically focusing on

505 peatland CO_2 emission hot spots remains limited (Anthony and Silver, 2023), despite increased

506 exploration of greenhouse gas emission hot spots in other ecosystems (e.g., agricultural field (Krichels

507 and Yang, 2019; Rey-Sanchez et al., 2022; Leifeld et al., 2020); wetland (Rey-Sanchez et al., 2022);

508 water-limited Mediterranean ecosystem (Leon et al., 2014); forest (Wangari et al., 2023)). Hence, to

509 improve the accuracy of CO_2 spatial budgeting for peatlands, there is a need for enhanced high-resolution

510 dynamic monitoring of hot spot areas (Becker et al., 2008). Our study demonstrates the great potential

511 of UAV technology for peatland hot spot identification and quantification, offering new insights into

512 studying soil respiration within heterogeneous ecosystems as well as optimizing peatland management

513 and CO_2 emission reduction strategies.

514

5 Conclusion

In this study, we monitored the dynamics of peatland surface and subsurface environments using both field surveys and multi-sensor UAVs at high spatial-temporal resolution. We investigated the influence of dynamic and static environmental factors on soil respiration rates across different scales, thereby enhancing our understanding of peatland carbon cycling. Additionally, we simulated CO_2 flux with high spatial-temporal resolution by integrating field measurements and UAV data. These reliable modelling allow us to identify and quantify CO_2 emission hot spots and hot moments across the landscape. To summarize, the main findings of our study are as follows:

(1) Soil respiration rates vary significantly across space and time, influenced by both dynamic and relatively static environmental factors at different scales. Temperature is the primary driver of CO_2 flux variations, explaining 33 % CO_2 seasonal variability and 18 % spatial variability. Soil moisture negatively affects both seasonal and spatial variations, accounting for 10 % - 11 % of the variance. Semi-dynamic factors (i.e., NDVI and root biomass) contribute 19 % to seasonal variability and 24 % to spatial variability. While relative static factors (i.e., the C/N and SOC stock) have little impact on the seasonal CO_2 flux variability, the contribution of the C/N ratio increases nearly 11 times for spatial variability.

(2) Predicting temporal series of hourly CO_2 flux can be effectively achieved (test set: $R^2 = 0.74$, $RMSE = 0.57$ μmol m^{-2} s^{-1}) by considering its relationship with key environmental variables such as air temperature, soil temperature and soil moisture, all of which are relatively straightforward to monitor. These reliable time series data provide a foundation for capturing respiration pulses occurring over short periods, with hot moments predominantly occurring in summer and early autumn.

(3) The UAV remote sensing data can yield robust spatial mapping of soil respiration rates across heterogeneous landscapes, with $RMSE$ and R^2 values of 0.54 μmol m^{-2} s^{-1} and 0.75 in the test dataset, respectively. These high-resolution CO_2 flux maps enable us to locate hot spots.

(4) Despite representing 10 % of time within one year, CO_2 fluxes from hot moments contribute 28 %-31 % to the overall CO_2 flux budgets. Approximately 10 % areas are identified as hot spots, while contributing 19.63 % ± 0.57 % of total CO_2 fluxes. The locations of high-frequency hot spots remain consistent, while the locations of sporadic hot spots vary over time.

542 **Code and data availability**

543 Code and data will be made available on request.

544

545 **CRediT authorship contribution statement**

546 **YL**: Writing – original draft, Visualization, Investigation, Formal analysis, Conceptualization. **MH**:

547 Writing – review & editing, Investigation. **AM**: Writing – review & editing. **SL**: Writing – review &

548 editing, Funding acquisition, Conceptualization. **SO**: Writing – review & editing, Funding acquisition,

549 Conceptualization. **VV**: Writing – review & editing, Funding acquisition, Conceptualization. **FJ**: Writing

550 – review & editing, Funding acquisition, Supervision, Conceptualization. **KVO**: Writing – review &

551 editing, Investigation, Funding acquisition, Supervision, Conceptualization.

552

553 **Declaration of Competing Interest**

554 The authors declare that they do not have any commercial or associative interest that represents a conflict

555 of interest in connection with the work submitted.

556

References

Abdalla, M., Hastings, A., Bell, M. J., Smith, J. U., Richards, M., Nilsson, M. B., Peichl, M., Löfvenius, M. O., Lund, M., Helfter, C., Nemitz, E., Sutton, M. A., Aurela, M., Lohila, A., Laurila, T., Dolman, A. J., Belelli-Marchesini, L., Pogson, M., Jones, E., Drewer, J., Drosler, M., and Smith, P.: Simulation of CO2 and Attribution Analysis at Six European Peatland Sites Using the ECOSSE Model, Water, Air, & Soil Pollution, 225, 2182, 10.1007/s11270-014-2182-8, 2014.

Acosta, M., Juszczak, R., Chojnicki, B., Pavelka, M., Havránková, K., Lesny, J., Krupková, L., Urbaniak, M., Machačová, K., and Olejnik, J.: CO2 Fluxes from Different Vegetation Communities on a Peatland Ecosystem, Wetlands, 37, 423-435, 10.1007/s13157-017-0878-4, 2017.

Anthony, T. L. and Silver, W. L.: Hot moments drive extreme nitrous oxide and methane emissions from agricultural peatlands, Global Change Biology, 27, 5141-5153, https://doi.org/10.1111/gcb.15802, 2021.

Anthony, T. L. and Silver, W. L.: Hot spots and hot moments of greenhouse gas emissions in agricultural peatlands, Biogeochemistry, 10.1007/s10533-023-01095-y, 2023.

Arias-Navarro, C., Díaz-Pinés, E., Klatt, S., Brandt, P., Rufino, M. C., Butterbach-Bahl, K., and Verchot, L. V.: Spatial variability of soil N2O and CO2 fluxes in different topographic positions in a tropical montane forest in Kenya, Journal of Geophysical Research: Biogeosciences, 122, 514-527, https://doi.org/10.1002/2016JG003667, 2017.

Azevedo, O., Parker, T. C., Siewert, M. B., and Subke, J.-A.: Predicting Soil Respiration from Plant Productivity (NDVI) in a Sub-Arctic Tundra Ecosystem, 10.3390/rs13132571, 2021.

Bates, D., Mächler, M., Bolker, B., and Walker, S.: Fitting Linear Mixed-Effects Models Using lme4, Journal of Statistical Software, 67, 1 - 48, 10.18637/jss.v067.i01, 2015.

Becker, T., Kutzbach, L., Forbrich, I., Schneider, J., Jager, D., Thees, B., and Wilmking, M.: Do we miss the hot spots? – The use of very high resolution aerial photographs to quantify carbon fluxes in peatlands, Biogeosciences, 5, 1387-1393, 10.5194/bg-5-1387-2008, 2008.

Bragazza, L., Parisod, J., Buttler, A., and Bardgett, R. D.: Biogeochemical plant–soil microbe feedback in response to climate warming in peatlands, Nature Climate Change, 3, 273-277, 10.1038/nclimate1781, 2013.

Briones, M. J. I., McNamara, N. P., Poskitt, J., Crow, S. E., and Ostle, N. J.: Interactive biotic and abiotic regulators of soil carbon cycling: evidence from controlled climate experiments on peatland and boreal

596   soils, Global Change Biology, 20, 2971-2982, https://doi.org/10.1111/gcb.12585, 2014.

597   Bubier, J. L., Bhatia, G., Moore, T. R., Roulet, N. T., and Lafleur, P. M.: Spatial and Temporal Variability

598   in Growing-Season Net Ecosystem Carbon Dioxide Exchange at a Large Peatland in Ontario, Canada,

599   Ecosystems, 6, 353-367, 10.1007/s10021-003-0125-0, 2003.

600   Cobb, A. R., Hoyt, A. M., Gandois, L., Eri, J., Dommain, R., Abu Salim, K., Kai, F. M., Haji Su'ut, N.

601   S., and Harvey, C. F.: How temporal patterns in rainfall determine the geomorphology and carbon fluxes

602   of tropical peatlands, Proceedings of the National Academy of Sciences, 114, E5187-E5196,

603   10.1073/pnas.1701090114, 2017.

604   Danevčič, T., Mandic-Mulec, I., Stres, B., Stopar, D., and Hacin, J.: Emissions of CO_2, CH_4 and N_2O

605   from Southern European peatlands, Soil Biology and Biochemistry, 42, 1437-1446,

606   https://doi.org/10.1016/j.soilbio.2010.05.004, 2010.

607   Deshmukh, C. S., Julius, D., Desai, A. R., Asyhari, A., Page, S. E., Nardi, N., Susanto, A. P., Nurholis,

608   N., Hendrizal, M., Kurnianto, S., Suardiwerianto, Y., Salam, Y. W., Agus, F., Astiani, D., Sabiham, S.,

609   Gauci, V., and Evans, C. D.: Conservation slows down emission increase from a tropical peatland in

610   Indonesia, Nature Geoscience, 14, 484-490, 10.1038/s41561-021-00785-2, 2021.

611   Dorrepaal, E., Toet, S., van Logtestijn, R. S. P., Swart, E., van de Weg, M. J., Callaghan, T. V., and Aerts,

612   R.: Carbon respiration from subsurface peat accelerated by climate warming in the subarctic, Nature,

613   460, 616-619, https://doi.org/10.1038/nature08216, 2009.

614   Evans, C. D., Peacock, M., Baird, A. J., Artz, R. R. E., Burden, A., Callaghan, N., Chapman, P. J., Cooper,

615   H. M., Coyle, M., Craig, E., Cumming, A., Dixon, S., Gauci, V., Grayson, R. P., Helfter, C., Heppell, C.

616   M., Holden, J., Jones, D. L., Kaduk, J., Levy, P., Matthews, R., McNamara, N. P., Misselbrook, T., Oakley,

617   S., Page, S. E., Rayment, M., Ridley, L. M., Stanley, K. M., Williamson, J. L., Worrall, F., and Morrison,

618   R.: Overriding water table control on managed peatland greenhouse gas emissions, Nature, 593, 548-552,

619   10.1038/s41586-021-03523-1, 2021.

620   Fang, C. and Moncrieff, J. B.: The dependence of soil CO_2 efflux on temperature, Soil Biology and

621   Biochemistry, 33, 155-165, https://doi.org/10.1016/S0038-0717(00)00125-5, 2001.

622   Farmer, J., Matthews, R., Smith, J. U., Smith, P., and Singh, B. K.: Assessing existing peatland models

623   for their applicability for modelling greenhouse gas emissions from tropical peat soils, Current Opinion

624   in Environmental Sustainability, 3, 339-349, https://doi.org/10.1016/j.cosust.2011.08.010, 2011.

625   Fernandez-Bou, A. S., Dierick, D., Allen, M. F., and Harmon, T. C.: Precipitation-drainage cycles lead

626   to hot moments in soil carbon dioxide dynamics in a Neotropical wet forest, Global Change Biology, 26,

627   5303-5319, 10.1111/gcb.15194, 2020.

628   Fox, J. and Monette, G.: Generalized Collinearity Diagnostics, Journal of the American Statistical

629   Association, 87, 178-183, https://doi.org/10.2307/2290467, 1992.

630   Frankard, P., Ghiette, P., Hindryckx, M.-N., Schumacker, R., and Wastiaux, C.: Peatlands of Wallony (S-

631   Belgium), SUO, Helsinki, Finland, 01/01, 33-37,

632   Frei, S., Knorr, K. H., Peiffer, S., and Fleckenstein, J. H.: Surface micro-topography causes hot spots of

633   biogeochemical activity in wetland systems: A virtual modeling experiment, Journal of Geophysical

634   Research: Biogeosciences, 117, https://doi.org/10.1029/2012JG002012, 2012.

635   García-García, A., Cuesta-Valero, F. J., Miralles, D. G., Mahecha, M. D., Quaas, J., Reichstein, M.,

636   Zscheischler, J., and Peng, J.: Soil heat extremes can outpace air temperature extremes, Nature Climate

637   Change, 13, 1237-1241, 10.1038/s41558-023-01812-3, 2023.

638   Harris, A. and Baird, A. J.: Microtopographic Drivers of Vegetation Patterning in Blanket Peatlands

639   Recovering from Erosion, Ecosystems, 22, 1035-1054, https://doi.org/10.1007/s10021-018-0321-6,

640   2019.

641   Hatala, J. A., Detto, M., Sonnentag, O., Deverel, S. J., Verfaillie, J., and Baldocchi, D. D.: Greenhouse

642   gas (CO_2, CH_4, H_2O) fluxes from drained and flooded agricultural peatlands in the Sacramento-San

643   Joaquin   Delta,   Agriculture,   Ecosystems   &   Environment,   150,   1-18,

644   https://doi.org/10.1016/j.agee.2012.01.009, 2012.

645   Henrion, M., Li, Y., Wu, K., Jonard, F., Opfergelt, S., Vanacker, V., Van Oost, K., and Lambot, S.: Drone-

646   Borne Ground-Penetrating Radar Reveals Spatiotemporal Moisture Dynamics in Peatland Root Zones,

647   Available at SSRN, http://dx.doi.org/10.2139/ssrn.5098978, 2025.

648   Hopple, A. M., Wilson, R. M., Kolton, M., Zalman, C. A., Chanton, J. P., Kostka, J., Hanson, P. J., Keller,

649   J. K., and Bridgham, S. D.: Massive peatland carbon banks vulnerable to rising temperatures, Nature

650   Communications, 11, 2373, 10.1038/s41467-020-16311-8, 2020.

651   Hoyos-Santillan, J., Lomax, B. H., Large, D., Turner, B. L., Boom, A., Lopez, O. R., and Sjögersten, S.:

652   Quality not quantity: Organic matter composition controls of CO_2 and CH_4 fluxes in neotropical peat

653   profiles, Soil Biology and Biochemistry, 103, 86-96, https://doi.org/10.1016/j.soilbio.2016.08.017, 2016.

Hoyt, A. M., Gandois, L., Eri, J., Kai, F. M., Harvey, C. F., and Cobb, A. R.: CO2 emissions from an undrained tropical peatland: Interacting influences of temperature, shading and water table depth, Global Change Biology, 25, 2885-2899, https://doi.org/10.1111/gcb.14702, 2019.

Huang, N., Gu, L., Black, T. A., Wang, L., and Niu, Z.: Remote sensing-based estimation of annual soil respiration at two contrasting forest sites, Journal of Geophysical Research: Biogeosciences, 120, 2306-2325, https://doi.org/10.1002/2015JG003060, 2015.

Huang, Y., Ciais, P., Luo, Y., Zhu, D., Wang, Y., Qiu, C., Goll, D. S., Guenet, B., Makowski, D., De Graaf, I., Leifeld, J., Kwon, M. J., Hu, J., and Qu, L.: Tradeoff of CO2 and CH4 emissions from global peatlands under water-table drawdown, Nature Climate Change, 11, 618-622, https://doi.org/10.1038/s41558-021-01059-w, 2021.

Ishikura, K., Darung, U., Inoue, T., and Hatano, R.: Variation in Soil Properties Regulate Greenhouse Gas Fluxes and Global Warming Potential in Three Land Use Types on Tropical Peat, 10.3390/atmos9120465, 2018.

Jovani-Sancho, A. J., Cummins, T., and Byrne, K. A.: Soil carbon balance of afforested peatlands in the maritime temperate climatic zone, Global Change Biology, 27, 3681-3698, https://doi.org/10.1111/gcb.15654, 2021.

Junttila, S., Kelly, J., Kljun, N., Aurela, M., Klemedtsson, L., Lohila, A., Nilsson, M. B., Rinne, J., Tuittila, E.-S., Vestin, P., Weslien, P., and Eklundh, L.: Upscaling Northern Peatland CO2 Fluxes Using Satellite Remote Sensing Data, 10.3390/rs13040818, 2021.

Juszczak, R., Humphreys, E., Acosta, M., Michalak-Galczewska, M., Kayzer, D., and Olejnik, J.: Ecosystem respiration in a heterogeneous temperate peatland and its sensitivity to peat temperature and water table depth, Plant and Soil, 366, 505-520, 10.1007/s11104-012-1441-y, 2013.

Kannenberg, S. A., Bowling, D. R., and Anderegg, W. R. L.: Hot moments in ecosystem fluxes: High GPP anomalies exert outsized influence on the carbon cycle and are differentially driven by moisture availability across biomes, Environmental Research Letters, 15, 054004, 10.1088/1748-9326/ab7b97, 2020.

Kelly, J., Kljun, N., Eklundh, L., Klemedtsson, L., Liljebladh, B., Olsson, P.-O., Weslien, P., and Xie, X.: Modelling and upscaling ecosystem respiration using thermal cameras and UAVs: Application to a peatland during and after a hot drought, Agricultural and Forest Meteorology, 300, 108330,

683   https://doi.org/10.1016/j.agrformet.2021.108330, 2021.

684   Kim, J. and Verma, S. B.: Soil surface CO2 flux in a Minnesota peatland, Biogeochemistry, 18, 37-51,

685   10.1007/BF00000425, 1992.

686   Knox, S. H., Sturtevant, C., Matthes, J. H., Koteen, L., Verfaillie, J., and Baldocchi, D.: Agricultural

687   peatland restoration: effects of land-use change on greenhouse gas (CO2 and CH4) fluxes in the

688   Sacramento-San Joaquin Delta, Global Change Biology, 21, 750-765, https://doi.org/10.1111/gcb.12745,

689   2015.

690   Krichels, A. H. and Yang, W. H.: Dynamic Controls on Field-Scale Soil Nitrous Oxide Hot Spots and

691   Hot Moments Across a Microtopographic Gradient, Journal of Geophysical Research: Biogeosciences,

692   124, 3618-3634, https://doi.org/10.1029/2019JG005224, 2019.

693   Kuzyakov, Y. and Blagodatskaya, E.: Microbial hotspots and hot moments in soil: Concept & review,

694   Soil Biology and Biochemistry, 83, 184-199, https://doi.org/10.1016/j.soilbio.2015.01.025, 2015.

695   Lees, K. J., Quaife, T., Artz, R. R. E., Khomik, M., and Clark, J. M.: Potential for using remote sensing

696   to estimate carbon fluxes across northern peatlands – A review, Science of The Total Environment, 615,

697   857-874, https://doi.org/10.1016/j.scitotenv.2017.09.103, 2018.

698   Leifeld, J. and Menichetti, L.: The underappreciated potential of peatlands in global climate change

699   mitigation strategies, Nature Communications, 9, 1071, 10.1038/s41467-018-03406-6, 2018.

700   Leifeld, J., Klein, K., and Wüst-Galley, C.: Soil organic matter stoichiometry as indicator for peatland

701   degradation, Scientific Reports, 10, 7634, 10.1038/s41598-020-64275-y, 2020.

702   Leifeld, J., Steffens, M., and Galego-Sala, A.: Sensitivity of peatland carbon loss to organic matter quality,

703   Geophysical Research Letters, 39, https://doi.org/10.1029/2012GL051856, 2012.

704   Leifeld, J., Wüst-Galley, C., and Page, S.: Intact and managed peatland soils as a source and sink of

705   GHGs from 1850 to 2100, Nature Climate Change, 9, 945-947, 10.1038/s41558-019-0615-5, 2019.

706   Leon, E., Vargas, R., Bullock, S., Lopez, E., Panosso, A. R., and La Scala, N.: Hot spots, hot moments,

707   and spatio-temporal controls on soil CO2 efflux in a water-limited ecosystem, Soil Biology and

708   Biochemistry, 77, 12-21, https://doi.org/10.1016/j.soilbio.2014.05.029, 2014.

709   Li, Y., Henrion, M., Moore, A., Lambot, S., Opfergelt, S., Vanacker, V., Jonard, F., and Van Oost, K.:

710   Factors controlling peat soil thickness and carbon storage in temperate peatlands based on UAV high-

711   resolution remote sensing, Geoderma, 449, 117009, https://doi.org/10.1016/j.geoderma.2024.117009,

712   2024.

713   Mason, C. W., Stoof, C. R., Richards, B. K., Das, S., Goodale, C. L., and Steenhuis, T. S.: Hotspots of

714   Nitrous Oxide Emission in Fertilized and Unfertilized Perennial Grasses, Soil Science Society of

715   America Journal, 81, 450-458, https://doi.org/10.2136/sssaj2016.08.0249, 2017.

716   McClain, M. E., Boyer, E. W., Dent, C. L., Gergel, S. E., Grimm, N. B., Groffman, P. M., Hart, S. C.,

717   Harvey, J. W., Johnston, C. A., Mayorga, E., McDowell, W. H., and Pinay, G.: Biogeochemical Hot Spots

718   and Hot Moments at the Interface of Terrestrial and Aquatic Ecosystems, Ecosystems, 6, 301-312,

719   10.1007/s10021-003-0161-9, 2003.

720   McNamara, N. P., Plant, T., Oakley, S., Ward, S., Wood, C., and Ostle, N.: Gully hotspot contribution to

721   landscape methane (CH4) and carbon dioxide (CO2) fluxes in a northern peatland, Science of The Total

722   Environment, 404, 354-360, https://doi.org/10.1016/j.scitotenv.2008.03.015, 2008.

723   Meehl, G. A. and Tebaldi, C.: More Intense, More Frequent, and Longer Lasting Heat Waves in the 21st

724   Century, Science, 305, 994-997, 10.1126/science.1098704, 2004.

725   Minasny, B., Berglund, Ö., Connolly, J., Hedley, C., de Vries, F., Gimona, A., Kempen, B., Kidd, D.,

726   Lilja, H., Malone, B., McBratney, A., Roudier, P., O'Rourke, S., Rudiyanto, Padarian, J., Poggio, L., ten

727   Caten, A., Thompson, D., Tuve, C., and Widyatmanti, W.: Digital mapping of peatlands – A critical

728   review, Earth-Science Reviews, 196, 102870, https://doi.org/10.1016/j.earscirev.2019.05.014, 2019.

729   Moore, P. A., Lukenbach, M. C., Thompson, D. K., Kettridge, N., Granath, G., and Waddington, J. M.:

730   Assessing the peatland hummock–hollow classification framework using high-resolution elevation

731   models: implications for appropriate complexity ecosystem modeling, Biogeosciences, 16, 3491-3506,

732   10.5194/bg-16-3491-2019, 2019.

733   Mormal, P. and Tricot, C.: Aperçu climatique des Hautes-Fagnes, Institut Royal météorologique de

734   Belgique, Brussel, 2004.

735   Murdoch, D. J. and Chow, E. D.: A Graphical Display of Large Correlation Matrices, The American

736   Statistician, 50, 178-180, https://doi.org/10.2307/2684435, 1996.

737   Nakagawa, S., Johnson, P. C. D., and Schielzeth, H.: The coefficient of determination R2 and intra-class

738   correlation coefficient from generalized linear mixed-effects models revisited and expanded, Journal of

739   The Royal Society Interface, 14, 20170213, 10.1098/rsif.2017.0213, 2017.

740   Nichols, D. S.: Temperature of upland and peatland soils in a north central Minnesota forest, Canadian

741   Journal of Soil Science, 78, 493-509, 10.4141/S96-030, 1998.

742   Pajula, R. and Purre, A.-H.: NDVI as a proxy to estimate the CO2 fluxes in peatlands: example of alkaline

743   fen, The 16th International Peatland Congress: Peatland and Peat - Source of Ecosystem Services, Tallinn,

744   Estonia,

745   Pinheiro, J. C. and Bates, D. M.: Fitting Linear Mixed-Effects Models, in: Mixed-Effects Models in S

746   and S-PLUS, edited by: Pinheiro, J. C., and Bates, D. M., Springer New York, New York, NY, 133-199,

747   10.1007/0-387-22747-4_4, 2000.

748   Prananto, J. A., Minasny, B., Comeau, L.-P., Rudiyanto, R., and Grace, P.: Drainage increases CO2 and

749   N2O emissions from tropical peat soils, Global Change Biology, 26, 4583-4600,

750   https://doi.org/10.1111/gcb.15147, 2020.

751   Rey-Sanchez, C., Arias-Ortiz, A., Kasak, K., Chu, H., Szutu, D., Verfaillie, J., and Baldocchi, D.:

752   Detecting Hot Spots of Methane Flux Using Footprint-Weighted Flux Maps, Journal of geophysical

753   research. Biogeosciences, 127, e2022JG006977, 10.1029/2022jg006977, 2022.

754   Rhoswen, L., Rhoswen, L., Nicholas, K., Nicholas, K., Devito, K. J., Kevin, J. D., Kevin, D., Richard,

755   M. P., Richard, M. P., Carl, M., Carl, A. M., Waddington, J. M., James, M. W., Stefan, K., and Stefan, K.:

756   Disturbance Impacts on Thermal Hot Spots and Hot Moments at the Peatland-Atmosphere Interface,

757   Geophysical Research Letters, 10.1002/2017gl075974, 2018.

758   Risk, D., Nickerson, N., Creelman, C., McArthur, G., and Owens, J.: Forced Diffusion soil flux: A new

759   technique for continuous monitoring of soil gas efflux, Agricultural and Forest Meteorology, 151, 1622-

760   1631, https://doi.org/10.1016/j.agrformet.2011.06.020, 2011.

761   Rowson, J., Worrall, F., Evans, M., and Dixon, S.: Predicting soil respiration from peatlands, Science of

762   The Total Environment, 442C, 397-404, 10.1016/j.scitotenv.2012.10.021, 2012.

763   Schubert, P., Eklundh, L., Lund, M., and Nilsson, M.: Estimating northern peatland CO2 exchange from

764   MODIS   time   series   data,   Remote   Sensing   of   Environment,   114,   1178-1189,

765   https://doi.org/10.1016/j.rse.2010.01.005, 2010.

766   Shrout, P. E. and Fleiss, J. L.: Intraclass correlations: Uses in assessing rater reliability, Psychological

767   Bulletin, 86, 420-428, 10.1037/0033-2909.86.2.420, 1979.

768   Simpson, G.: Drivers of peatland CO_2 balance: a fusion of UAV remote sensing and micrometeorology,

769   Doctoral dissertation, School of GeoSciences, The University of Edinburgh, U.K., 57-157 pp.,

770   http://dx.doi.org/10.7488/era/3228, 2023.

771   Sougnez, N. and Vanacker, V.: The topographic signature of Quaternary tectonic uplift in the Ardennes

772   massif (Western Europe), Hydrol. Earth Syst. Sci., 15, 1095-1107, https://doi.org/10.5194/hess-15-1095-

773   2011, 2011.

774   Steenvoorden, J., Bartholomeus, H., and Limpens, J.: Less is more: Optimizing vegetation mapping in

775   peatlands using unmanned aerial vehicles (UAVs), International Journal of Applied Earth Observation

776   and Geoinformation, 117, 103220, https://doi.org/10.1016/j.jag.2023.103220, 2023.

777   Stoy, P. C., Street, L. E., Johnson, A. V., Prieto-Blanco, A., and Ewing, S. A.: Temperature, Heat Flux,

778   and Reflectance of Common Subarctic Mosses and Lichens under Field Conditions: Might Changes to

779   Community Composition Impact Climate-Relevant Surface Fluxes?, Arctic, Antarctic, and Alpine

780   Research, 44, 500-508, 10.1657/1938-4246-44.4.500, 2012.

781   Swails, E. E., Ardón, M., Krauss, K. W., Peralta, A. L., Emanuel, R. E., Helton, A. M., Morse, J. L.,

782   Gutenberg, L., Cormier, N., Shoch, D., Settlemyer, S., Soderholm, E., Boutin, B. P., Peoples, C., and

783   Ward, S.: Response of soil respiration to changes in soil temperature and water table level in drained and

784   restored peatlands of the southeastern United States, Carbon Balance and Management, 17, 18,

785   10.1186/s13021-022-00219-5, 2022.

786   Treat, C. C., Wollheim, W. M., Varner, R. K., Grandy, A. S., Talbot, J., and Frolking, S.: Temperature and

787   peat type control CO_2 and CH_4 production in Alaskan permafrost peats, Global Change Biology, 20,

788   2674-2686, 10.1111/gcb.12572, 2014.

789   Turetsky, M. R., Benscoter, B., Page, S., Rein, G., van der Werf, G. R., and Watts, A.: Global vulnerability

790   of peatlands to fire and carbon loss, Nature Geoscience, 8, 11-14, 10.1038/ngeo2325, 2015.

791   UNEP: Global Peatlands Assessment – The State of the World's Peatlands: Evidence for action toward

792   the conservation, restoration, and sustainable management of peatlands, Global Peatlands Initiative,

793   United   Nations   Environment   Programme9789280739916,   125-154,

794   https://doi.org/10.59117/20.500.11822/41222, 2022.

795   van Giersbergen, Q., Barthelmes, A., Couwenberg, j., Fritz, C., Lång, K., Martin, N., and Tanneberger,

796   F.: Identifying hotspots of greenhouse gas emissions from drained peatlands in the European Union,

797   PREPRINT (Version 1) available at Research Square, https://doi.org/10.21203/rs.3.rs-4629642/v1, 2024.

798   Walcker, R., Le Lay, C., Gandois, L., Elger, A., and Jassey, V. E. J.: High-resolution mapping of peatland

799   CO2 fluxes using drone multispectral images, Ecological Informatics, 103060,

800   https://doi.org/10.1016/j.ecoinf.2025.103060, 2025.

801   Walker, T. N., Garnett, M. H., Ward, S. E., Oakley, S., Bardgett, R. D., and Ostle, N. J.: Vascular plants

802   promote ancient peatland carbon loss with climate warming, Global Change Biology, 22, 1880-1889,

803   https://doi.org/10.1111/gcb.13213, 2016.

804   Wang, H., Richardson, C. J., and Ho, M.: Dual controls on carbon loss during drought in peatlands,

805   Nature Climate Change, 5, 584-587, 10.1038/NCLIMATE2643, 2015a.

806   Wang, H., Tian, J., Chen, H., Ho, M., Vilgalys, R., Bu, Z.-J., Liu, X., and Richardson, C. J.: Vegetation

807   and microbes interact to preserve carbon in many wooded peatlands, Communications Earth &

808   Environment, 2, 67, 10.1038/s43247-021-00136-4, 2021.

809   Wang, M., Moore, T. R., Talbot, J., and Riley, J. L.: The stoichiometry of carbon and nutrients in peat

810   formation, Global Biogeochemical Cycles, 29, 113-121, https://doi.org/10.1002/2014GB005000, 2015b.

811   Wangari, E. G., Mwangada Mwanake, R., Houska, T., Kraus, D., Gettel, G. M., Kiese, R., Breuer, L.,

812   and Butterbach-Bahl, K.: Identifying landscape hot and cold spots of soil greenhouse gas fluxes by

813   combining field measurements and remote sensing data, Biogeosciences, 20, 5029-5067, 10.5194/bg-20-

814   5029-2023, 2023.

815   Wangari, E. G., Mwanake, R. M., Kraus, D., Werner, C., Gettel, G. M., Kiese, R., Breuer, L., Butterbach-

816   Bahl, K., and Houska, T.: Number of Chamber Measurement Locations for Accurate Quantification of

817   Landscape-Scale Greenhouse Gas Fluxes: Importance of Land Use, Seasonality, and Greenhouse Gas

818   Type, Journal of Geophysical Research: Biogeosciences, 127, e2022JG006901,

819   https://doi.org/10.1029/2022JG006901, 2022.

820   Webster, K. L., Creed, I. F., Beall, F. D., and Bourbonnière, R. A.: Sensitivity of catchment-aggregated

821   estimates of soil carbon dioxide efflux to topography under different climatic conditions, Journal of

822   Geophysical Research: Biogeosciences, 113, https://doi.org/10.1029/2008JG000707, 2008.

823   Wilkinson, S. L., Andersen, R., Moore, P. A., Davidson, S. J., Granath, G., and Waddington, J. M.:

824   Wildfire and degradation accelerate northern peatland carbon release, Nature Climate Change, 13, 456-

825   461, https://doi.org/10.1038/s41558-023-01657-w, 2023.

826   Wilson, D., Dixon, S. D., Artz, R. R. E., Smith, T. E. L., Evans, C. D., Owen, H. J. F., Archer, E., and

827   Renou-Wilson, F.: Derivation of greenhouse gas emission factors for peatlands managed for extraction

828   in the Republic of Ireland and the United Kingdom, Biogeosciences, 12, 5291-5308, 10.5194/bg-12-

829   5291-2015, 2015.

830   Wright, E. L., Black, C. R., Turner, B. L., and Sjögersten, S.: Environmental controls of temporal and

831   spatial variability in and fluxes in a neotropical peatland, Global Change Biology, 19, 3775-3789,

832   https://doi.org/10.1111/gcb.12330, 2013.

833   Wutzler, T., Perez-Priego, O., Morris, K., El-Madany, T. S., and Migliavacca, M.: Soil CO2 efflux errors

834   are lognormally distributed – implications and guidance, Geosci. Instrum. Method. Data Syst., 9, 239-

835   254, 10.5194/gi-9-239-2020, 2020.

836   Xu, J., Morris, P. J., Liu, J., and Holden, J.: PEATMAP: Refining estimates of global peatland distribution

837   based on a meta-analysis, CATENA, 160, 134-140, https://doi.org/10.1016/j.catena.2017.09.010, 2018.

838   Yu, Z., Loisel, J., Brosseau, D. P., Beilman, D. W., and Hunt, S. J.: Global peatland dynamics since the

839   Last Glacial Maximum, Geophysical Research Letters, 37, https://doi.org/10.1029/2010GL043584, 2010.

840   Zhang, C., Comas, X., and Brodylo, D.: A Remote Sensing Technique to Upscale Methane Emission

841   Flux in a Subtropical Peatland, Journal of Geophysical Research: Biogeosciences, 125, e2020JG006002,

842   https://doi.org/10.1029/2020JG006002, 2020.

843   Zou, J., Ziegler, A. D., Chen, D., McNicol, G., Ciais, P., Jiang, X., Zheng, C., Wu, J., Wu, J., Lin, Z., He,

844   X., Brown, L. E., Holden, J., Zhang, Z., Ramchunder, S. J., Chen, A., and Zeng, Z.: Rewetting global

845   wetlands effectively reduces major greenhouse gas emissions, Nature Geoscience, 15, 627-632,

846   10.1038/s41561-022-00989-0, 2022.

847